Editors' Suggestion   Featured in Physics

Intermittent versus continuous swimming: An optimization tale

Gen Li ⓞ*

Japan Agency for Marine-Earth Science and Technology (JAMSTEC), 3173-25, Showa-machi,
Kanazawa-ku, Yokohama-city, Kanagawa, 236-0001, Japan

Dmitry Kolomenskiy ⓞ

Center for Materials Technologies (CMT), Skolkovo Institute of Science and Technology,
Bolshoy Boulevard 30, Building 1, Moscow 121205, Russia

Hao Liu ⓞ

Graduate School of Engineering, Chiba University, 1-33, Yayoicho, Inage-ku, Chiba-shi,
Chiba 263-8522, Japan

Ramiro Godoy-Diana ⓞ and Benjamin Thiria

Laboratoire de Physique et Mécanique des Milieux Hétérogènes (PMMH), CNRS UMR 7636,
ESPCI Paris—PSL University, Sorbonne Université, Université Paris Cité, 75005 Paris, France

Intermittent swimming, also termed "burst-and-coast swimming," has been reported as a strategy for fish to enhance their energetical efficiency. Intermittent swimming involves additional control parameters, which complexifies its understanding by means of quantitative and parametrical analysis, in comparison with continuous swimming. In this study, we used a hybrid computational fluid dynamic (CFD) model to assess the swimming performance in intermittent swimming parametrically and quantitatively. A Navier-Stokes solver is applied to construct a database in the multidimensional space of the control parameters to connect the undulation kinematics to swimming performance. Based on the database, an indirect numerical approach named "gait assembly" is used to generate arbitrary burst-and-coast gaits to explore the parameter space. Our simulations directly measured the hydrodynamics and energetics under the unsteady added-mass effect during burst-and-coast swimming. The results suggest that the instantaneous power of burst is basically determined by undulatory kinematics. The results show that the energetical performance of burst-and-coast swimming can be better than that of continuous swimming, but also that an unoptimized burst-and-coast gait may become very energetically expensive. These results shed light on the mechanisms at play in intermittent swimming, enabling us to better understand fish behavior and to propose design guidelines for fishlike robots.

I. INTRODUCTION

Undulatory propulsion is commonly adopted by fish in their locomotion [1,2]. A great number of biomechanical and physiological studies on fish locomotion are based on a cyclic swimming state, where continuous undulation enables fish to maintain steady cruising velocity and energy expenditure [3]. On the other hand, like many other animals, fish may also perform intermittent

---

*ligen@jamstec.go.jp
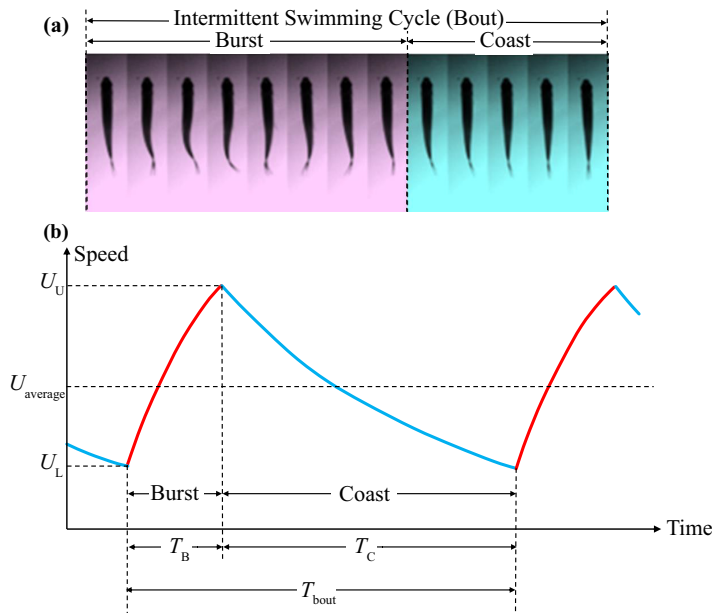
FIG. 1. Features of burst-and-coast swimming. (a) Example observation on burst-and-coast swimming. (b) Schematic description of burst-and-coast swimming with regard to time and velocity, revised from Videler and Weihs [10].

locomotion [4,5]. The intermittent locomotion may be applied in predator-prey interaction, sensing, habitat assessment, and cruising motion [5–8]. Intermittent locomotion in fish swimming is also termed burst-and-coast swimming, which is a two-phase periodic behavior consisting of an active propulsive phase followed by a passive gliding phase with the body straightened [4,9]. As shown in Fig. 1(a), during the burst phase, the fish undulates its body and caudal fin to gain forward momentum, while during the coast phase, the fish keeps its body straight and consumes its forward momentum for traveling distance. By repeating the burst-and-coast process, the average swimming velocity can be sustained at a desired level.

Since the pioneering studies by Weihs *et al.* [9,10], intermittent swimming has been investigated from the biomechanical perspective. Intermittent swimming is considered as a means to improve the energetic performance in linear swimming (e.g., [9–11]). A theoretical basis is provided by the "Bone-Lighthill boundary-layer thinning hypothesis" [3], according to which, the lateral motion of a fish body element may reduce the thickness of the boundary layer, and thus increase the friction drag. Propulsive movement of the body and appendages is expected to increase the drag by a factor of 2–5 [3,12–14]. Thus, by ceasing its body undulation a fish may exploit the lower drag of a rigid body and eventually reduce the energy consumed to overcome drag [15]. Such advantages are confirmed by experiment and simulation [12,16–18]. It has been hypothesized that the advantage of an intermittent swimming strategy mainly benefits BCF (body and caudal fin) swimmers using subcarangiform and carangiform swimming, as MPF (median-paired fin) swimmers and, to a lesser extent, thick-bodied thunniform swimmers already maintain a rigid body; thus little advantage would be gained by adopting burst-and-coast swimming [19]. An analytical study by Blake [20] reports that the frequent burst-and-coast swimmers are characterized by a fineness ratio (the ratio of the length of a body to its maximum width) around 5, and that fish with lower fineness ratios use less burst-and-coast swimming. Nevertheless, in a computational fluid dynamic study by Xia *et al.* [21], they report that an energetic improvement in the burst-and-coast swimming of virtual thunniform swimmers is possible (our remarks on this study are discussed in Sec. IV A).

Burst-and-coast swimming gait and performance are also correlated with the cruising velocity. Our most recent experimental-numerical study shows that fish are able to optimize their gait for minimal cost of transport, by modulating a unique intrinsic cycle to sustain the demanded velocity [22]. Interestingly, a few recent studies report that in some circumstances intermittent swimming may cost more energy than cyclic swimming (e.g., [23,24]), which suggests the energy-saving function of burst-and-coast swimming is not inevitable and may require optimization in control parameters. Overall, since the hydrodynamic details of burst-and-coast swimming are usually hard to access by experimental measurement, and the intermittent behavior is associated to a complex control parameter space, there is a strong lack of quantitative and parametrical analyses concerning intermittent swimming.

The purpose of this paper is to parametrically assess the swimming performance in intermittent swimming and to compare the performance of intermittent and continuous swimming patterns. To accurately examine the highly dynamic instantaneous performance during burst-and-coast swimming, we use a direct computational fluid dynamic (CFD) model of a self-propelled fish based on the Navier-Stokes equations [14,25,26]. To parametrically explore the gait and its corresponding swimming performance in intermittent swimming, we use an indirect numerical approach named "gait assembly" [22], which generates arbitrary intermittent gaits based on the database constructed by multiple direct CFD simulations. The rest of this paper is organized as follows: In Sec. II we investigate the hydrodynamic characteristics of burst-and-coast swimming using a Navier-Stokes solver; in Sec. III, we optimize the burst-and-coast gait based on the database constructed in Sec. II and explore the parameter space. We investigate the optimal gait in burst-and-coast swimming and make a comparison with a continuous swimming gait. Note that the numerical methods used in Secs. II and III are, respectively, explained in the first subsection of each section. Comparison between our results and previous studies, as well as inspirations for future research, are discussed in Sec. IV.

II. HYDRODYNAMIC MODELING OF BURST-AND-COAST SWIMMING

A. Numerical approach in this section

We use a previously validated three-dimensional computational fluid dynamic (CFD) approach based on an overset-grid finite-volume method to simulate a self-propelled model fish [25–27] (for more information including the numerical validation, see the Supplemental Material (SM) [28]). The model fish swims freely in the horizontal plane [three degrees of freedom (DoF), including translational motion in the horizontal plane and rotation about the vertical axis]. The approach comprises surface models of a typical carangiform fish shape [Fig. 2(a), model fish body length: 2 cm, dimension in CFD mesh: 121×97], and local fine-scale body-fitted grids plus a large stationary global grid [Fig. 2(c)] to calculate the flow patterns around the fish with sufficient resolution. As shown in Fig. 2(b), the instantaneous body shape is driven by sinusoidal variation of the midline, cf. [26],

$$H(l, t) = \alpha l^2 \, \sin\left(\frac{2\pi l}{\lambda} - 2\pi f t\right), \tag{1}$$

where l is the dimensionless distance from the snout along the longitudinal axis of the fish based on the length of the fish model L; $H(l, t)$ is the dimensionless lateral excursion in a frame attached to the fish head at time t; α is the dimensionless amplitude control factor; λ is the length of the body wave. Since we simulate a carangiform swimmer [1] and the wavelength of a typical carangiform swimmer is approximately equivalent to or greater than $1L$ [29], we define $\lambda = 1.1L$; f is the tail-beat frequency. This equation may cause total body length along the midline to vary during the tail beat, which is corrected by a procedure that preserves the lateral excursion $H(l, t)$ and ensures constant body length (see SM, Sec. B 3 [28]).

Three-dimensional Navier-Stokes (NS) equations in an inertial frame of reference are solved. The solving process is implemented using the finite-volume method (FVM), based on a multiblock,

(a) Surface model
(b) Kinematics
$$H(l,t) = \alpha \, l^2 \sin\left(\frac{2\pi l}{\lambda} - 2\pi f t\right)$$

$0 \qquad 0.5 \qquad 1\,(L)$

(c) Body-fitted grid

Global grid

(d) CFD results

Direct simulation

Database
Burst × 40
Coast × 1

Gait Assembly (Indirect numerical approach)

(e) speed

U_U

time-sequence
of speed in burst

U_L

power

time-sequence
of power in burst

speed

time-sequence
of speed in coast

time

power

time-sequence
of power in coast

time

speed

U_U

U_L

power

assembled time-
sequence of speed

assembled time-
sequence of power

burst-and-coast bout

FIG. 2. Numerical methods. (Upper) Direct numerical approach: (a) Fish surface model; (b) kinematic model; (c) computational mesh; (d) an example of CFD flow field. (Lower) (e) Indirect numerical approach: Burst-and-coast gait assembly.

an overset-mesh system, and an interblock communication algorithm. The governing equations for the fluid solution are the three-dimensional, incompressible and unsteady NS equations written in strongly conservative form for mass and momentum [27]. To accelerate the computation and improve the robustness during iteration, the artificial compressibility method is adopted by adding a pseudotime derivative of pressure to the continuity equation [27]. For further details of the NS solver, see SM, Sec. B [28].

While the deformation of the central body axis of the fish is prescribed, the center-of-mass (CoM) movements and body orientation are determined by the hydrodynamic and inertial forces generated by the swimming model fish. The forces acting on the body and its motion are obtained through coupling the hydrodynamic and body dynamic solutions, which ensures that the motions of the fish correspond to the hydrodynamic and inertial forces exerted on the fish. The range of Reynolds

numbers in this study is below 6000, turbulence models are not used, and the grid resolution at Re = 6000 has been justified in our previous study [30].

A swimming fish generates unsteady pressure and shear stress at all locations on its body. The shear component of the stress predominantly converts into skin friction drag, while the pressure component of the stress, particularly in the posterior fish body, changes its direction rapidly during fish undulation. Hence, in this study, the instantaneous thrust (drag) at each time step is defined as the sum of the forward (backward) components of pressure and shear stress over all fish surface elements (see SM, Fig. S4 [28]). Each surface element could contribute to thrust or drag at different time steps even within one tail-beat cycle, as well as to thrust and drag simultaneously (e.g., generating pressure-based thrust and shear-based drag). Such definition may effectively separate thrust and drag forces during unsteady, undulatory swimming.

In this paper, power refers to "mechanical power," defined as the sum of the hydrodynamic and body inertial powers:

$$P = P_{\text{hydro}} + P_{\text{body}}. \tag{2}$$

Hydrodynamic power is calculated as the sum of the hydrodynamic work on the body surface, such that

$$P_{\text{hydro}} = \oiint^{\text{surface}} (\mathbf{f} \cdot \mathbf{U}) dS, \tag{3}$$

where P_{hydro} is the hydrodynamic power; ds denotes the surface element; $\mathbf{f}$ is the hydrodynamic stress vector acting on the surface element; $\mathbf{U}$ is the velocity vector on this surface element.

Body inertial power is computed as the sum of the kinetic energy change rate of all body elements (inside the body), such that

$$P_{\text{body}} = \oiiint^{\text{body}} (\rho \cdot \mathbf{a} \cdot \mathbf{U}) dV, \tag{4}$$

where P_{body} is the body inertial power; dV denotes body volume element; $\mathbf{a}$ and $\mathbf{U}$ are the acceleration and velocity vectors of each body volume element, respectively; and ρ is the local density.

Note that based on Eq. (2), during the coast phase, the mechanical power is zero.

The dimensionless cost of transport (CoT) is defined as

$$\Omega^* = \frac{E}{mgS}, \tag{5}$$

where E denotes energy consumption, m denotes body mass, g denotes gravitational acceleration, and S denotes traveled distance.

B. Hydrodynamics and energetics of a nonrepeated burst-and-coast bout

Using the Navier-Stokes solver introduced in Sec. II A, we simulated a nonrepeated swimming bout consisting of developed burst and coast phases (Fig. 3; see Supplemental Video in the SM [28]). As shown in Figs. 3 and 4(a), the fish started swimming from rest [body axis 0 in Fig. 4(a)] with a body deformation driven by Eq. (1) at $f = 10$ Hz, $\alpha = 0.11$, based on experimental observations [29,31]. The cyclic swimming continued for 15 tail-beat cycles [until body axis 15 in Fig. 4(a)] at the end of which the fish had accelerated to a nominally terminal velocity, then stopped its undulation [body axis 15.5 in Fig. 4(a)] and the fish body was kept straight. The fish coasted for another 1.5 s, slowing down until almost reaching a full stop [body axis 30 in Fig. 4(a)]. The flow field produced by this burst-and-coast bout is shown by Fig. 3 (see Supplemental Video in the SM [28]): The fish generated jet flows and vortex rings behind itself. Corresponding to the sharp acceleration at the beginning, those initial jets merged into a strong backward jet (① in Fig. 3). As the acceleration rate decreased, the lateral velocity components gradually dominated the jet flows (② in Fig. 3). On
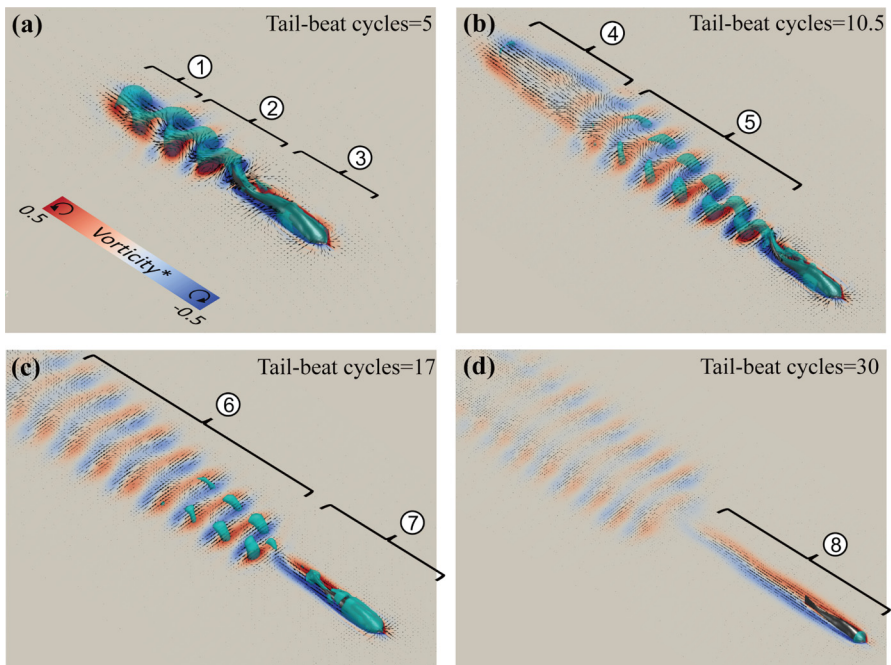
FIG. 3. Flow field features of a nonrepeated burst-and-coast bout. The burst of cyclic swimming lasts for 15 tail-beat cycles during which the fish has accelerated to a relatively stable velocity. It then stops its undulation and the fish body is kept straight during the coast phase that lasts for another 1.5 s (equivalent to a 15 tail-beat cycle time), reaching an almost static condition. Flow features are marked by numbers and explained in the text. Panels (a–d) correspond to 5, 10.5, 17, and 30 tail-beat cycles, respectively.

the fish body, the anterior part was rigid and surrounded by relatively stable boundary vorticity—a shear layer surrounding the fish body. At the posterior body, the surrounding boundary vorticity was disturbed due to the undulation, and vortices shed in a staggered pattern (③ in Fig. 3) similar to the observation by Wu *et al.* [12]. As the fish swam further, those starting jets merged into a large backward jet zone (④ in Fig. 3). Unlike the early vortices that merged into two main vortices, those vortices generated later were in a staggered pattern (⑤ and ⑥ in Fig. 3). The angle between the vortex ring axis and the backward direction (opposite to the swimming direction) was observed to change—early vortex rings generated during sharp acceleration have smaller angles, while vortex rings generated during stable swimming contain a larger portion of lateral velocity component, which agreed with the observation by Akanyeti *et al.* [32]. When the fish stopped undulating and began to coast, its tail stopped shedding staggered-pattern vortices, and the entire body produced an elongated boundary vorticity layer (⑦ in Fig. 3) that covered the gliding trajectory of the fish (⑧ in Fig. 3).

The undulation formed periodic fluctuations in velocity, power, thrust, and drag time sequences [gray curves in Figs. 4(b), 4(d), 4(f), and 4(h)]. These fluctuations were low pass filtered (LOWPASS function, MATLAB R2020b, cutoff frequency = f) to clearly demonstrate the average trend of those performance parameters [black curves in Figs. 4(b), 4(d), 4(f), and 4(h)]. As shown in Fig. 4(b), in the burst phase, the acceleration was rapid at the beginning, with a sharp increase of fish swimming velocity, but it attenuated to zero as the drag matched the thrust. In the coast phase, as the fish stopped undulating, its velocity dropped sharply at the beginning of the coasting phase and then the deceleration rate weakened as the velocity decreased. The shape of the velocity curve [Fig. 4(b)], consisting of a gently sloped top of the burst phase and a gently sloped bottom of the coast phase, agreed with the theoretical investigation by Videler and Weihs [10]. The trend of this velocity curve
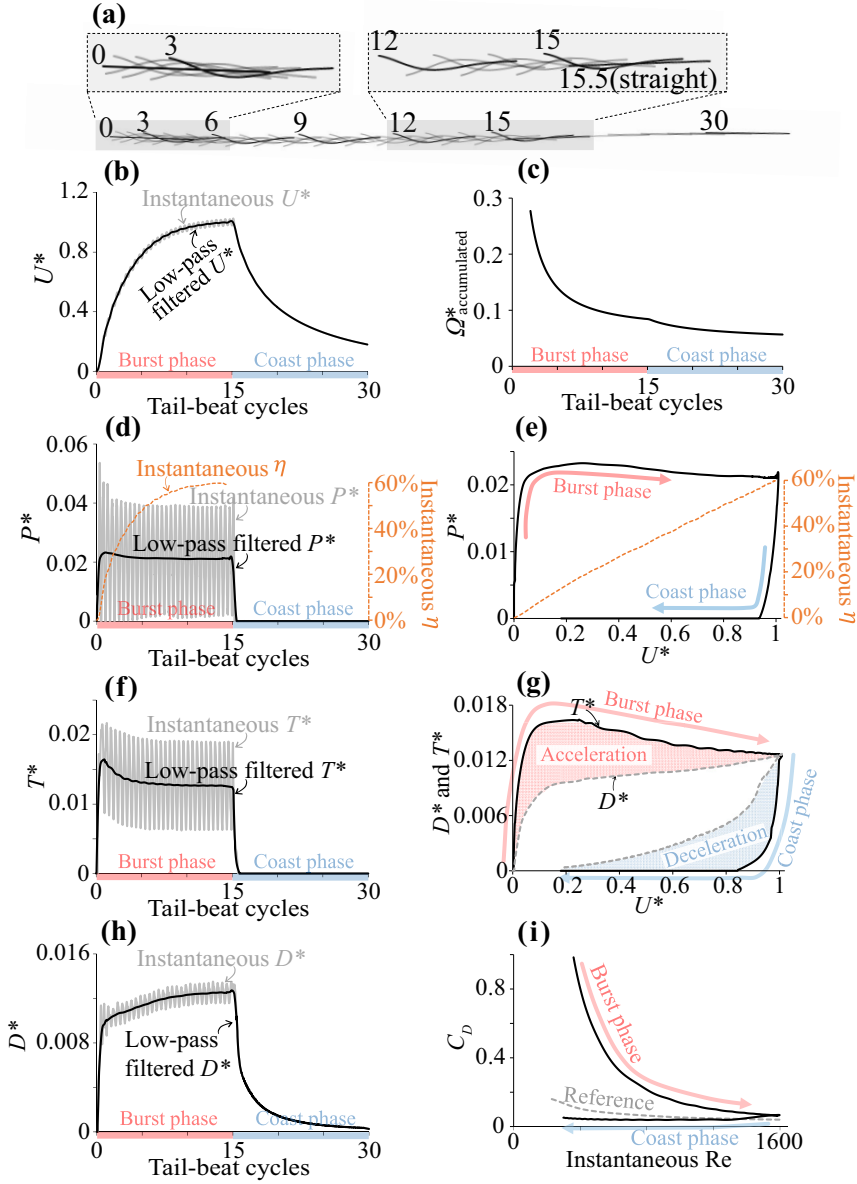
FIG. 4. Simulation results of a single burst-and-coast bout. (a) Body axis time sequences; (b) U^* versus tail-beat cycles; (c) $\Omega^*_{\text{accumulated}}$; (d) P^* and η versus tail-beat cycles; (e) P^* and η versus U^*; (f) T^* versus tail-beat cycles; (g) T^* and D^* versus U^*; (h) D^* versus tail-beat cycles; (i) drag coefficient C_D. In (i), as a reference, a speed-specific drag coefficient curve of the fish steadily gliding with a straight body is presented by the gray dashed line. Note that this reference curve does not represent a dynamic process. Each point on the reference curve denotes a drag coefficient obtained in a simulation when the fish constantly glides at a given speed. (U^*: Dimensionless velocity, defined as $U^* = U/U_{\text{ref}}$; P^*: Dimensionless power, defined as $P^* = P/(\rho U_{\text{ref}}^3 L^2)$; T^*: Dimensionless thrust, defined as $T^* = T/(\rho U_{\text{ref}}^2 L^2)$; D^*: Dimensionless drag, defined as $D^* = D/(\rho U_{\text{ref}}^2 L^2)$; C_D: Drag coefficient, defined as $C_D = 2D/(\rho U^2 S)$; P: Instantaneous power; ρ: The water density; U: Instantaneous velocity; U_{ref}: The reference velocity, defined as the velocity at the end of burst, $3.9L/\text{s}$; L: The body length; S: The wetted area; T: Instantaneous thrust; D: Instantaneous drag; P: Instantaneous power; η: Froude efficiency, where $\eta = TU/P$.

was determined by the characteristics of the thrust and drag of the swimming fish. The thrust of the fish, as shown by Fig. 4(f), was most strong at the beginning of the burst phase, then gradually decreased as swimming velocity increased. During the coast phase, the thrust immediately dropped to zero as the undulation ceased. The drag on the fish showed positive correlation with the swimming velocity [Fig. 4(h)]; however, at one specific velocity, the magnitude of drag differed dramatically between the burst and coast phases, since the undulatory propulsion amplified the magnitude of drag [9].

In Fig. 4(i), a drag coefficient curve is drawn to demonstrate the dynamic change in drag during burst-and-coast swim (black solid curve, which is further decomposed into two parts respectively formed by the burst and coast phases). As a reference, a velocity-specified drag coefficient curve of a fish steadily gliding with a straight body is added to the plot (gray dashed line). The ratio between the instantaneous drag coefficients of burst-and-coast swim and steady glide, defined as drag amplifying factor β, was not a constant value as applied in previous analytical research (e.g., [10]), but varied in a wide range. At the beginning of the burst phase, $\beta \approx 10$, representing a strong amplification in drag due to added-mass effect; at the end of the burst phase, β gradually diminished to approximately 2, representing that the added-mass effect is attenuated as the magnitude of acceleration diminishes, while a certain extent of drag amplification was still maintained due to the body undulation; as the fish transited to coasting, β quickly became less than 1, which means that during the coast phase the added-mass effect was reversed, resulting in a lower drag than that observed in a steady glide with the same velocity.

As shown in Fig. 4(g), during the burst phase, a stabilized velocity condition was achieved as the decreasing thrust and the increasing drag balanced at a specific velocity. In the coast phase, thrust dropped immediately to zero due to the absence of undulation; meanwhile, the drag also dropped sharply but not to zero because the fish moving body had to overcome the hydrodynamic drag and decelerated.

As to the power [Fig. 4(e)], it is worth noting that during the burst the relation between power and forward-swimming velocity differed much from that in steady swimming: The power is not proportional to velocity, instead, it rises to a maximum level immediately when the fish starts the burst, and is slightly reduced as the velocity increases, reaching a relatively stable level at a specific velocity. The power during the burst seems to be not strongly influenced by the instantaneous velocity. Apparently, the lateral undulating velocity mattered most for the power expenditure during the early stage of burst, rather than the forward component of the CoM velocity. In the coast phase, the power dropped immediately to zero.

The simulation results show that, during the burst, the fish had to spend extra effort to overcome the added-mass effect and lateral-side power expenditure. Here, we define the accumulated cost of transport to represent the cost of transport from the start to present time t_p:

$$\Omega^*_{\text{accumulated}}(t_p) = \frac{E(t_p)}{mgS(t_p)} = \frac{\int_0^{t_p} P(t)dt}{mg \int_0^{t_p} U(t)dt},$$

where $E(t_p)$ denotes the accumulated energy consumption from the beginning to present time t_p; $S(t_p)$ denotes the accumulated traveled distance from the beginning to present time t_p. As shown in Fig. 4(c), $\Omega^*_{\text{accumulated}}$ started extremely high at the beginning of the burst phase, then decreased as the velocity approaches the equilibrium state. This shows that, in this burst-and-coast process, fish invest extra energy during the burst phase, and earn the benefit during the coast phase.

C. Instantaneous velocity and power during the burst phase

In this section, our analysis focuses on the swimming performance during the burst phase. By using the Navier-Stokes solver introduced in Sec. II A, we directly simulated 40 burst-swimming processes from rest to full velocity under various undulatory kinematics: The combinations of tail-beat frequency (2, 6, 10, 14, and 18 Hz) and amplitude [α = 0.02, 0.06, 0.08, 0.10, 0.12, 0.14, 0.18, and 0.22 in Eq. (1)]. In all burst-swimming processes, as the fish sufficiently accelerates itself and
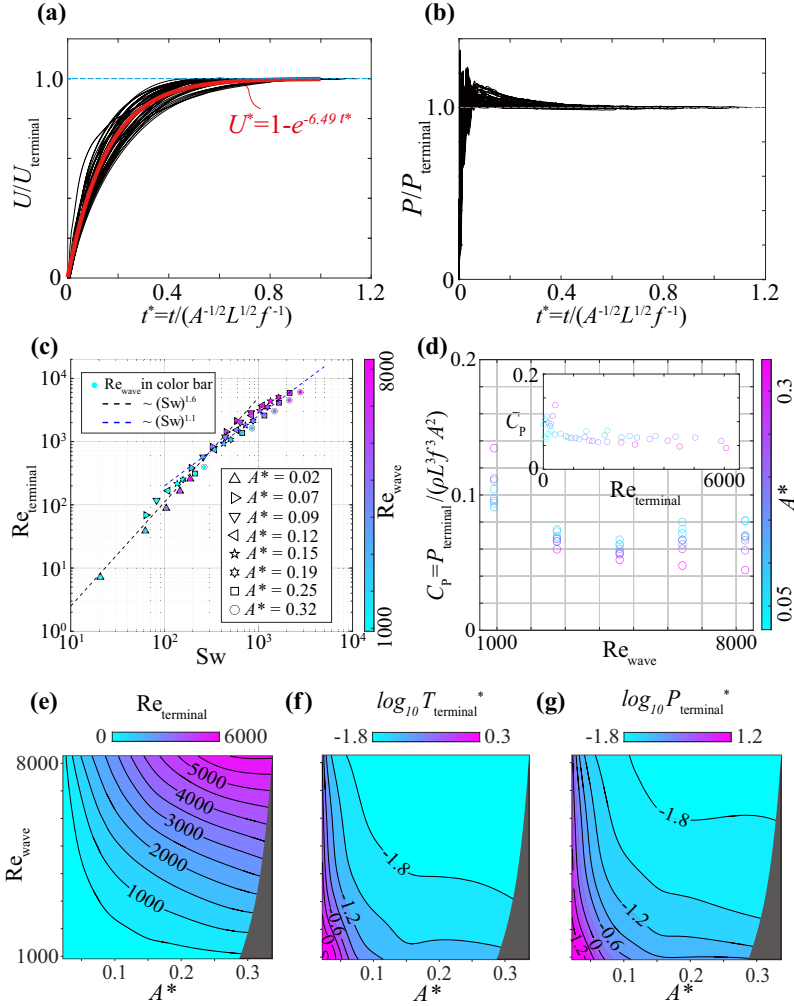
FIG. 5. Simulation results in 40 full burst simulations with various undulatory kinematics: The combinations between tail-beat frequency and amplitude. (a) Relationship between instantaneous velocity and dimensionless time for all burst simulations, where the dimensionless instantaneous velocity in each simulation is normalized by the terminal velocity $U_{terminal}$. (b) Relationship between instantaneous power and dimensionless time in all burst simulations, where the instantaneous dimensionless power in each simulation is normalized by the terminal power $P_{terminal}$. The dimensionless time in (a,b) is given by $t^* = t/(A^{-1/2}L^{1/2}f^{-1})$. (c) Relationship between Sw, Re_{wave}, and $Re_{terminal}$ in burst simulations, where $Sw = fAL/\nu$, $Re_{wave} = fL^2/\nu$, $A^* = A/L$, and $Re_{terminal} = UL/\nu$. (d) Relationship between dimensionless burst-undulation frequency Re_{wave} and power coefficient $[C_P = P_{terminal}/(\rho L^3 f^3 A^2)]$; the relationship between $Re_{terminal}$ and C_P is also shown in the inset; (e) $Re_{terminal}$ map in the Re_{wave}-A^* plane; (f) $T_{terminal}^*$ map in the Re_{wave}-A^* plane; (g) $P_{terminal}^*$ map in the Re_{wave}-A^* plane. (e–g) are recalculated from Li *et al.* [14]. The dimensional data of all burst simulations are shown in the SM, Sec. D [28].

approaches the cyclic regime, its thrust, velocity, and power are termed terminal thrust, velocity, and power, respectively.

We obtained the time profiles of the forward-swimming velocity and hydrodynamic power, which are shown, respectively, in Figs. 5(a) and 5(b) in the normalized form $U/U_{terminal}$ and $P/P_{terminal}$ as functions of the dimensionless time $t^* = t/(A^{*-1/2}f^{-1})$, where $A^* = A/L$. Normalization with the

values U_{terminal} and P_{terminal} that correspond to the end-point values in each transient reveals the shapes of typical time profiles of U and P. In Fig. 5(a), considering the velocity curves passing from the origin and asymptotically approaching $U^* = U/U_{\text{terminal}} = 1$, we attempted to use an exponential function $U^*(t^*) = 1 - e^{a\,t^*}(a < 0)$ to fit the average of all those burst curves. We obtained an exponential fit line that accurately represents the acceleration process in burst swim:

$$U^*(t^*) = 1 - e^{-6.49\,t^*}. \tag{6}$$

In Fig. 5(b), power curves also form a common pattern: The power rises sharply at the very initial stage of burst, and after that, though the fish is still accelerating, the power curves are predominantly constant. The results suggest that when the kinematics is specified, the burst-swimming velocity and power are basically determined by the burst-undulation kinematics (in this study, tail-beat frequency and amplitude). We emphasize that the instantaneous power during the burst is not determined by the instantaneous swimming velocity. Our results suggest that the velocity during a burst can be approximated by an exponential fit line $U^*(t^*) = 1 - e^{a\,t^*}$ $(a < 0)$, while the power during the entire burst can be approximated by a constant value equal to the terminal power.

The magnitude of U_{terminal} and P_{terminal} vary across the cases in a wide range, but Figs. 5(c) and 5(d) suggest that both can be approximated as simple functions of tail-beat frequency and amplitude. In Fig. 5(c), $\text{Re}_{\text{terminal}} \propto \text{Sw}^k$, where $\text{Re}_{\text{terminal}} = U_{\text{terminal}}L/\nu$ and $\text{Sw} = fAL/\nu$ (ν: Kinematic viscosity) is the swimming number, defined as k ranges dynamically between 1.1 and 1.6, for which Gazzola *et al.* [33] derive $k = 4/3$ at low Re and $k = 1$ at high Re. Figure 5(d) demonstrates that P_{terminal} was, in the majority of cases, reasonably well characterized by a constant value of the power coefficient $C_P = 0.65$, where $C_P = P_{\text{terminal}}/\rho L^3 f^3 A^2$. In Fig. 5(d), the wave-speed-based Reynolds number was defined as $\text{Re}_{\text{wave}} = fL^2/\nu$. Large values of C_P in Fig. 5(d) correspond to those cases where Re_{wave} and $\text{Re}_{\text{terminal}}$ [the inset in Fig. 5(d)] are small. The maps of $\text{Re}_{\text{terminal}}$, T_{terminal}, and P_{terminal} in the $\text{Re}_{\text{wave}} - A^*$ plane are shown in panels (e–g), respectively.

III. OPTIMIZATION IN BURST-AND-COAST SWIMMING

A. Algorithm of burst-and-coast gait assembly and optimization

Fish usually perform an intermittent swimming gait formed by repeated burst-and-coast bouts, which determines a multidimensional control parameter space. The control parameters can be limited to four: The tail-beat frequency f during burst swim, the tail-beat amplitude A during burst swim, an upper velocity boundary U_U [transitional point from coast to burst, Fig. 1(b)], and a lower velocity boundary U_L [transitional point from coast to burst, Fig. 1(b)]. Fully covering this four-dimensional parameter space by direct simulations is impractical. To reduce the complexity in the parametric analysis, we assume the following:

Assumptions for burst-and-coast gait assembly algorithm:

(1) A burst-and-coast bout can be considered as assembled by a burst phase and a coast phase. The two phases share the same upper and lower velocity boundaries, while the hydrodynamics of each phase is independent.

(2) The swimming performance in the burst phase is determined by the burst kinematics, i.e., the tail-beat frequency and amplitude. A burst phase with velocity range from U_L to U_U can be regarded as a part trimmed from a full burst process with a velocity range from 0 to U_{terminal} ($U_{\text{terminal}} \geqslant U_U$).

(3) The coast phase is completely passive. The instantaneous drag only depends on the instantaneous velocity. Thus, an arbitrary coast phase with velocity ranges from U_U to U_L can be regarded as a part trimmed from a coast process covering a sufficiently large velocity range.

(4) The transitions between burst and coast phases are immediate and can be neglected.

As shown in Fig. 2(e), based on these assumptions, we designed an indirect numerical approach, which uses a database of 41 direct simulations (40 bursts and one coast) to assemble arbitrary burst-and-coast gaits. The parameter space was scanned with coarse resolution to find burst-and-

coast gaits satisfying the specific velocity requirements, and then further determined the optimal burst-and-coast gait corresponding to minimal CoT.

According to the analysis in Sec. III C, the instantaneous velocity during a burst using the tail-beat frequency f and amplitude A can be approximated as

$$U_{\text{burst}}(t) = U_{\text{terminal}}(f, A)\left(1 - e^{-6.49t/(A^{-1/2}L^{1/2}f^{-1})}\right), \tag{7}$$

where $U_{\text{terminal}}(f, A)$ is the terminal velocity of a burst. As to the instantaneous power during the burst, based on the instantaneous power data shown in Fig. 5(c), it is reasonable to approximate the instantaneous power by the terminal power of the burst as

$$P_{\text{burst}}(t) = P_{\text{terminal}}(f, A). \tag{8}$$

We mapped $U_{\text{terminal}}(f, A)$ and $P_{\text{terminal}}(f, A)$ in Fig. 5, so that U_{terminal} and P_{terminal} of any arbitrary burst process can be quantified by interpolation. According to Eqs. (7) and (8), the instantaneous velocity and power can be further calculated.

On the other hand, in coast swimming, the to-be-trimmed coast process was obtained by a single direct simulation, by letting the model fish stop undulating after reaching a velocity higher than the highest velocity reached by all 40 burst processes. During this coast phase, the body was held straight, and the fish decelerated until the velocity dropped to almost zero. The mechanical power consumption during the coast phase was assumed to be zero.

The full swimming cycle is obtained by concatenating the trimmed burst-and-coast time sequences [Fig. 2(e)]. The procedure is then duplicated to produce a sawtooth-wave time profile of the velocity. For a given set of the four parameters (f, α, U_U, and U_L), as long as U_U and U_L are within the possible velocity range of a "full burst process," a unique burst-and-coast swimming gait can be obtained. The average velocity of the generated burst-and-coast swimming gait is defined as U_{average} and is calculated numerically by the following equation:

$$U_{\text{average}} = \frac{\int_0^{t_{\text{B}}} U_{\text{burst}}(t)dt + \int_0^{t_{\text{C}}} U_{\text{coast}}(t)dt}{t_{\text{B}} + t_{\text{C}}}. \tag{9}$$

The cost of transport of the assembled burst-and-coast gait is defined as follows:

$$\Omega^* = \frac{\int_0^{t_{\text{B}}} P_{\text{burst}}(t)dt}{mg\left(\int_0^{t_{\text{B}}} U_{\text{burst}}(t)dt + \int_0^{t_{\text{C}}} U_{\text{coast}}(t)dt\right)}. \tag{10}$$

In order to find an optimal burst-and-coast swimming gait that would meet the required average velocity U_{average} with the lowest cost of transport, we programmed code within MATLAB to scan the four parameter dimensions (f: Scan resolution 0.1 Hz; scan range 2–18 Hz; A: Scan resolution 0.0015L; range approximately 0.02–0.32L; the scan resolution in U_U and U_L is less than 10^{-7} L/s). To rule out unrealistically short burst-and-coast bouts, in the simulation we require that the burst time is long enough to complete at least one tail-beat stroke, while the coast time is long enough to skip at least one tail-beat stroke; i.e., $T_B \geqslant 0.5/f$ and $T_C \geqslant 0.5/f$.

For further details of the scan algorithm, see the SM, Sec. C [28].

B. Optimal gait and performance in burst-and-coast swimming

By using the above-mentioned gait assembly approach, we specified optimal burst-and-coast gaits with minimal CoT. As shown by the circles (○) in Figs. 6(a) and 6(b), the burst-phase frequency of the optimal burst-and-coast gait, represented by Re$_{\text{wave}}$, increased with the mean speed, while the optimal peak-to-peak tail-beat amplitude of the optimal burst-and-coast gait appears to be relatively stable at around 0.16L. Between frequency and amplitude, fish in burst-and-coast gait seem to use frequency as the primary means of control. Figure 6(c) demonstrates that the optimal upper and lower speed bounds, U_U and U_L, respectively, monotonically increase with the average speed. We

(a) Optimal tail-beat frequency

(b) Optimal tail-beat amplitude

(c) Upper and lower boundaries of velocity in burst-and-coast gait

(d) Optimal cost of transport (COT)
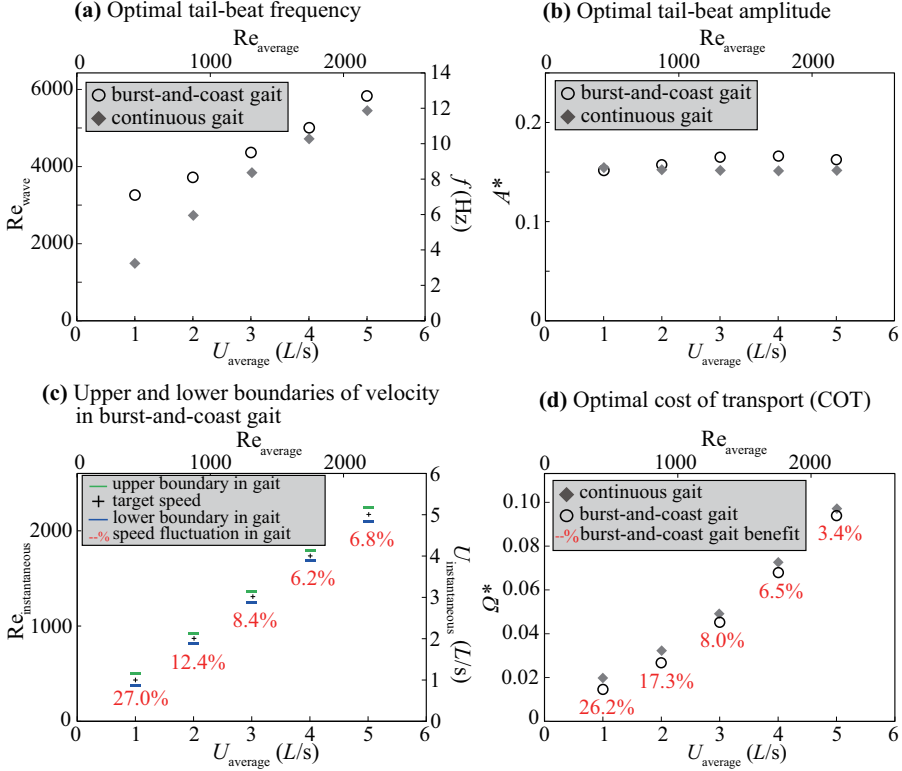
FIG. 6. Comparison between optimal burst-and-coast and continuous gaits at various speed levels. (a) Optimal tail-beat frequency; (b) optimal tail-beat amplitude; (c) upper and lower speed boundaries of optimal burst-and-coast swimming, and the fluctuation range around the average speed. Note that upper and lower velocity boundaries are not applicable for the continuous gait. (d) Cost of transport of optimal burst-and-coast gait and continuous gait. $1 L/s = 0.02$ m/s.

calculated the ratio of velocity fluctuation as follows:

$$\delta = \frac{U_U - U_L}{U_{\text{average}}} \times 100\%. \tag{11}$$

At lower speed (1 L/s) δ was about 27%. In the medium- and high-speed regime, δ became narrower as speed increases, decreasing to about 7% at 5 L/s. Overall, the ratio of velocity fluctuation was less than 30% and tended to become narrower as average speed increased.

C. Burst-and-coast versus continuous swimming

This subsection quantitatively compares the optimal kinematics and energetic performance between burst-and-coast and continuous swimming gaits. Here, optimization was also required for the continuous swimming gait for each target speed level. The cost of transport of cyclic swimming was calculated as

$$\Omega^* = \frac{P_\infty(f, A)}{mgU_\infty(f, A)}, \tag{12}$$

where P_∞ and U_∞ are, respectively, the velocity and power of cyclic swimming using the kinematics defined by (f, A), which are, respectively, equivalent to $P_{\text{terminal}}(f, A)$ and $U_{\text{terminal}}(f, A)$ in Figs. 5(f)

and 5(g). The optimization consisted in finding a minimal $\frac{P_\infty(f,A)}{U_\infty(f,A)}$ when $U_\infty(f, A)$ equals the target speed level, which has been calculated in Li *et al.* (Fig. 2 in Li *et al.* [14]) and we adopted the results.

The results of the optimal continuous undulation gait are shown in Fig. 6 by a rhombus (♦). The predicted optimal frequency of the continuous undulation gait basically rose as the target speed increased [Fig. 6(a)]. Compared with the optimal frequency of the burst-and-coast gait, the optimal frequency of the continuous gait was relatively lower. Especially, at the very low velocity of 1 *L*/s, the continuous gait merely used half the frequency of that used in the burst-and-coast gait. The optimal tail-beat amplitude of the continuous gait appeared to be also constant, and very similar to that of the burst-and-coast gait [Fig. 6(b)].

Figure 6(d) shows the comparison of the predicted optimal CoT values between the burst-and-coast gait and the continuous swimming gait. It is noteworthy that, at all speed levels, the optimized burst-and-coast gait required a lower CoT than that of the continuous undulation gait. In the meantime, our results show that the relative reduction of the CoT by the burst-and-coast gait was most significant at lower speeds, and became less significant as the speed increased [Fig. 6(d)]. As the speed increased, the optimal burst-and-coast gait approached the optimal continuous gait in many aspects.

D. Nonoptimized burst-and-coast gaits may be energetically inefficient

The simulation also shows that nonoptimized burst-and-coast gaits result in a rather wide range of CoT values. When scanning the parameter space by the gait assembly approach, we also obtained extremely large CoT at each velocity levels. The "bad" kinematics corresponding to extremely high CoT generally occurs near the boundary of the parameter space, with both extremely large tail-beat frequency or amplitude (at all velocity levels, maximal-CoT burst-and-coast gaits use extreme kinematic values: Maximal *f* and *A* in the scanned range).

In Fig. 7(a), the CoT of nonoptimized burst-and-coast gaits can be several times higher than the minimal CoT at each velocity level, especially at lower velocity regimes, where the ratio between maximum and minimum CoT can be up to almost 8. The maximum CoT of the burst-and-coast gait is also much higher than that of the optimal continuous gait, indicating that when the gait is not sufficiently optimized, the energetical efficiency of burst and coast could be more expensive than that of the continuous swimming gait. To provide an example to demonstrate typical "good" and "bad" burst-and-coast gaits, we present the velocity time sequences of the optimal and the "worst" burst-and-coast gaits at target speed $U_{\text{target}} = 3$ *L*/s in Fig. 7(b). Inefficient burst-and-coast gaits were generally characterized by a wide velocity interval (between lower and upper velocity boundaries) and large bout time, and used extremely high tail-beat frequencies and amplitudes in the burst phase. The fish accelerated to terminal speed and then coasted for a long period to fully exhaust the momentum. On the contrary, in the optimal burst-and-coast gait, the velocity interval was narrow and the bout time was much shorter. Optimal burst-and-coast gaits used moderate tail-beat frequency and amplitude, and the velocity time sequences fluctuated around the average speed.

IV. DISCUSSION

A. Different understanding from previous investigations

In contrast with most previous studies in the comparison of energetical performance between burst-and-coast and continuous swimming gaits, we have in the present work ensured that (1) the comparison is based on the same velocity [17], and (2) both burst-and-coast and continuous gaits are optimized parametrically. We consider that these two principles deliver a fair comparison between burst-and-coast and continuous gaits. These principles, to some extent, narrow the difference between the energetical performance between burst-and-coast and continuous gaits, in contrast with previous studies reporting a 50%–60% energy saving by adopting burst-and-coast swimming [9,18]. It is worth noting that, for both burst-and-coast and continuous gaits, the mechanical CoT is

(a) CoT range at various target velocity levels

(b) Gait examples at $U_{\text{target}}=3L/s$ (Re=1377)
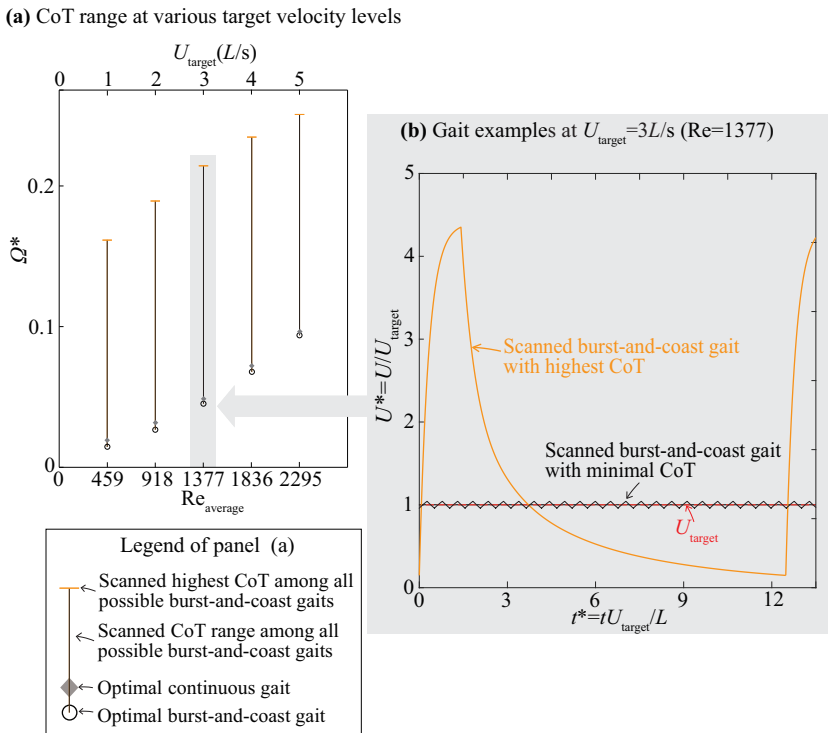
FIG. 7. Optimal gaits at various target velocity levels with burst-and-coast and continuous gaits, as well as information about the worst burst-and-coast gaits scanned. (a) Optimal cost of transport in burst-and-coast gait (○) and continuous gait (♦), as well as the CoT range between optimal and worst burst-and-coast gaits scanned. (b) Examples of scanned optimal and worst burst-and-coast gaits at $U_{\text{target}} = 3L/s$. The worst gait adopted an extremely powerful burst to reach a high velocity and then coasted for a long period to exhaust momentum.

positively correlated to swimming speed. Therefore, when we compare the energetical performance between burst-and-coast and continuous swimming gaits we ensure that both are measured at the same swimming speed. This requirement, together with the carangiform kinematics and moderate Reynolds number, led us to a different conclusion from what Xia *et al.* [21] found in their study that focused on thunniform swimming. Our direct simulation of a self-propelled fish reveals details of the hydrodynamics of burst-and-coast swimming. It shows that the burst-and-coast gait may save energy mainly because the ratio of undulatory-body drag to straight-body drag at a specific velocity is greater than 1 (i.e., $\beta > 1$), which agrees with the understanding of previous analytical models [9]. However, our simulation also demonstrates the complexity of the β value, which changes rapidly during acceleration and transition between burst and coast. In particular, β is relatively large at the early stage of the burst [Fig. 4(i)], hence estimating β as a constant seems inaccurate. Furthermore, the CFD prediction demonstrates that the instantaneous power of the burst phase does not follow a proportional relationship with instantaneous velocity. Instead, it sustains at a constant magnitude determined by the kinematics, which may be approximated by the power of the continuous cyclic swimming under the same undulation kinematics. For both β and instantaneous power issues, our CFD simulations show that the burst phase is more energetically expensive than anticipated from previous analytical models.

This study provides insight into the roles of control parameters during the highly unsteady burst process. As shown by the typical time profiles of U and P in Fig. 5(a) based on the definition

of dimensionless t^*, the increment in both tail-beat amplitude and frequency can enhance the acceleration toward the terminal velocity (i.e., the rate of $U/U_{terminal}$ approaches 1). Comparing tail-beat frequency and amplitude, tail-beat frequency plays a relatively stronger role than tail-beat amplitude in acceleration. Li *et al.* [22] quantitatively showed that the choice of tail-beat amplitude can cause changes in swimming drag, as predicted by the Bone-Lighthill hypothesis, which forces fish to find a proper tail-beat amplitude to maintain the effectiveness in propulsion while avoiding causing excessive drag. Such strategy can extend to the unsteady burst-and-coast. Thus, a fish in burst phase still tends to keep a steady tail-beat amplitude level and adjust tail-beat frequency to control swimming velocity.

B. Limitations of the current approach

The indirect numerical approach (i.e., the "gait assembly" algorithm), was used in our previous study to analyze the burst-and-coast gait observed experimentally in the station-keeping swimming of rummy-nose tetrafish [22]. For moderate to high velocities ($U > 1$ BL/s), the parameters that minimize the energy cost of swimming closely match the experimental data; however, the prediction at low-velocity regimes diverges from the observations. The gait assembly algorithm is a compromise approach to explore the four-dimensional parameter space at a feasible cost. The primary source of error in the gait assembly algorithm is the absence of the transition process between the burst and coast phases, while neglecting the fluctuation of the velocity and power is also an important factor of error. The gait assembly algorithm only assembled smoothed velocity trajectories. To examine how the forces and powers differ from direct CFD under the gait assembly assumptions, two testing CFD cases are conducted, respectively, at speeds of $1L$/s and $3L$/s in the SM, Sec. E [28]. According to this comparison between CFD and the gait assembly algorithm, the latter appears, despite its imperfections, to be a reasonable method to explore the highly complex parameter space of the burst-and-coast swimming. To further improve the accuracy and reliability in future works, massive computational resources are needed. Also, beyond the scope of this paper, an optimization algorithm with machine learning that would optimize the strategy parametrically based on both real-time simulation and a historically accumulated database may provide an interesting perspective. Recent works on the optimization in fish collective swimming based on machine learning [34,35] provide examples.

Our numerical approach focused on hydrodynamic consumption and neglected physiological consumption. A difference exists between metabolic consumption and hydrodynamic consumption—the former is higher because of the basal metabolic consumption (the rate of energy expenditure at rest is not zero) and the lossy conversion of chemical into mechanical energy [36,37]. As explained by Li *et al.* [14], when physiological contributions are included in the consideration, the relation between metabolic consumption and speed is likely U shaped [37,38]; thus a global optimal swimming velocity for cruising can be found, whereas when physiological contributions are neglected in a computational fluid dynamic investigation, the relation between metabolic consumption and speed is basically monotonic and thus a global optimal swimming velocity cannot be found. Therefore, the current CFD approach can only be used to optimize kinematics at a specified speed, but cannot be used to find a global optimal speed with minimal metabolic cost, unless CFD approaches are combined with models representing the basal metabolic consumption and the conversion of chemical energy into mechanical work by the swimming musculature in the future.

C. Advices for robot fish design

The Bone-Lighthill hypothesis is a basis of the energy-saving mechanism of the burst-and-coast swimming. Hence the optimal burst-and-coast gait obtained in this study may only apply to undulatory (or flapping) swimmers. It remains to be verified if a burst-and-coast propulsive mode

can be applied to rigid-body swimmers, such as propeller-driven autonomous underwater vehicles (AUVs), where changes in drag between the bursting and coasting phases might be negligible.

It should be mentioned that, in a realistic situation, the burst-and-coast parameters may change over the course of a swimming trajectory with the changing environment and navigation objectives. The gait assembly approach is justified if the timescale of those variations is longer than the burst-and-coast bout time. Indeed, swimming trajectories consist of approximately constant gait sequences when fish forage [39] or swim in a stream [22]. The gait assembly approximation may not be suitable for analyzing rapid maneuvering or strong external perturbations, but these situations are of interest from the viewpoint of stability and control rather than energy efficiency.

Our results suggest that, for fishlike robots, the mechanical power during acceleration may be approximated by the power during continuous cyclic swimming with the same undulation kinematics. So far, the burst-and-coast style of locomotion can be realized by fishlike robots and artificial swimmer designs [40,41]. This research demonstrates that the energy-saving function in a burst-and-coast gait is feasible. Nonetheless, it also warns that unoptimized burst-and-coast gaits may be extremely inefficient, with energetical efficiency much worse than the continuous gait with the same velocity, which partly agrees with a numerical study by Ashraf *et al.* [24]. Therefore, when introducing the burst-and-coast swimming to fishlike robot systems, developers ought to be aware that burst-and-coast swimming does not necessarily lead to energy saving, and be cautious when choosing the burst-and-coast gait. As suggested by Fig. 7, a burst-and-coast gait with short bout time and small velocity interval may be relatively more economical than a burst-and-coast gait with long bout time and large velocity interval.

[1] M. Sfakiotakis, D. M. Lane, and J. B. C. Davies, Review of fish swimming modes for aquatic locomotion, IEEE J. Oceanic Eng. **24**, 237 (1999).

[2] J. R. Hunter and J. R. Zweifel, Swimming speed, tail beat frequency, tail beat amplitude, and size in jack mackerel, *Trachurus symmetricus*, and other fishes, Fish. Bull. **69**, 253 (1971).

[3] M. J. Lighthill, Large-amplitude elongated-body theory of fish locomotion, Proc. R. Soc. London, Ser. B **179**, 125 (1971).

[4] J. J. Videler, *Fish Swimming*, 10th ed. (Springer Science & Business Media, Berlin, 1993).

[5] D. L. Kramer and R. L. McLaughlin, The behavioral ecology of intermittent locomotion, Am. Zool. **41**, 137 (2001).

[6] S. P. Windsor, D. Tan, and J. C. Montgomery, Swimming kinematics and hydrodynamic imaging in the blind Mexican cave fish (*Astyanax fasciatus*), J. Exp. Biol. **211**, 2950 (2008).

[7] A. P. Soto and M. J. McHenry, Pursuit predation with intermittent locomotion in zebrafish, J. Exp. Biol. **223**, jeb230623 (2020).

[8] A. McKee, A. P. Soto, P. Chen, and M. J. McHenry, The sensory basis of schooling by intermittent swimming in the rummy-nose tetra (*Hemigrammus rhodostomus*): Schooling by intermittent swimming, Proc. R. Soc. B **287**, 20200568 (2020).

[9] D. Weihs, Energetic advantages of burst swimming of fish, J. Theor. Biol. **48**, 215 (1974).

[10] J. J. Videler and D. Weihs, Energetic advantages of burst-and-coast swimming of fish at high speeds J. Exp. Biol. **97**, 169 (1982).

[11] J. J. Videler, Swimming movements, body structure and propulsion in cod *Gadus morhua*, Symp. Zool. Soc. London **48**, 1 (1981).

[12] G. Wu, Y. Yang, and L. Zeng, Kinematics, hydrodynamics and energetic advantages of burst-and-coast swimming of koi carps (*Cyprinus carpio koi*), J. Exp. Biol. **210**, 2181 (2007).

[13] E. J. Anderson, W. R. McGillis, and M. A. Grosenbaugh, The boundary layer of swimming fish, J. Exp. Biol. **204**, 81 (2001).

[14] G. Li, H. Liu, U. K. Müller, C. J. Voesenek, and J. L. van Leeuwen, Fishes regulate tail-beat kinematics to minimize speed-specific cost of transport, Proc. R. Soc. B **288**, 20211601 (2021).

[15] D. Webb and P. W. Weihs, *Fish Biomechanics* (Praeger, New York, 1983).

[16] D. Floryan, T. Van Buren, and A. J. Smits, Forces and energetics of intermittent swimming, Acta Mech. Sin. **33**, 725 (2017).

[17] L. Dai, G. He, X. Zhang, and X. Zhang, Intermittent locomotion of a fish-like swimmer driven by passive elastic mechanism, Bioinspir. Biomim. **13**, 056011 (2018).

[18] E. Akoz and K. W. Moored, Unsteady propulsion by an intermittent swimming gait, J. Fluid Mech. **834**, 149 (2018).

[19] F. E. Fish, Swimming strategies for energy economy, in *Fish Locomotion. An Eco-ethological Perspective*, edited by P. Domenici and B. G. Kapoor (Taylor & Francis, New York, 2010), pp. 90–122.

[20] R. W. Blake, Functional design and burst-and-coast swimming in fishes, Can. J. Zool. **61**, 2491 (1983).

[21] D. Xia, W.-S. Chen, J.-k. Liu, and X. Luo, The energy-saving advantages of burst-and-glide mode for thunniform swimming, J. Hydrodyn. **30**, 1072 (2018).

[22] G. Li, I. Ashraf, B. François, D. Kolomenskiy, F. Lechenault, R. Godoy-Diana, and B. Thiria, Burst-and-coast swimmers optimize gait by adapting unique intrinsic cycle, Commun. Biol. **4**, 40 (2021).

[23] P. Han, J. Wang, and H. Dong, Effects of intermittent swimming gait in fish-like locomotion, in *AIAA Scitech 2020 Forum*, AIAA 2020-1779 (AIAA, Reston, VA, 2020), Part F.

[24] I. Ashraf, S. van Wassenbergh, and S. Verma, Burst-and-coast swimming is not always energetically beneficial in fish (*Hemigrammus bleheri*), Bioinspiration Biomimetics **16**, 16002 (2021).

[25] G. Li, U. K. Müller, J. L. van Leeuwen, and H. Liu, Body dynamics and hydrodynamics of swimming fish larvae: A computational study, J. Exp. Biol. **215**, 4015 (2012).

[26] G. Li, U. K. Müller, J. L. van Leeuwen, and H. Liu, Fish larvae exploit edge vortices along their dorsal and ventral fin folds to propel themselves, J. R. Soc. Interface **13**, 20160068 (2016).

[27] H. Liu, Integrated modeling of insect flight: From morphology, kinematics to aerodynamics, J. Comput. Phys. **228**, 439 (2009).

[28] See Supplemental Material at http://link.aps.org/supplemental/10.1103/PhysRevFluids.8.013101 for information about methodology and supplemental computational results, and a movie of burst-and-coast simulation, which also includes Refs. [42,43].

[29] C. Wardle, J. Videler, and J. Altringham, Tuning in to fish swimming waves: Body form, swimming mode and muscle function, J. Exp. Biol. **198**, 1629 (1995).

[30] G. Li, U. K. Müller, J. L. van Leeuwen, and H. Liu, Escape trajectories are deflected when fish larvae intercept their own C-start wake, J. R. Soc. Interface **11**, 20140848 (2014).

[31] G. Li, D. Kolomenskiy, H. Liu, B. Thiria, and R. Godoy-Diana, On the energetics and stability of a minimal fish school, PLoS ONE **14**, e0215265 (2019).

[32] O. Akanyeti, J. Putney, Y. R. Yanagitsuru, G. V. Lauder, W. J. Stewart, and J. C. Liao, Accelerating fishes increase propulsive efficiency by modulating vortex ring geometry, Proc. Natl. Acad. Sci. USA **114**, 13828 (2017).

[33] M. Gazzola, M. Argentina, and L. Mahadevan, Scaling macroscopic aquatic locomotion, Nat. Phys. **10**, 758 (2014).

[34] S. Verma, G. Novati, and P. Koumoutsakos, Efficient collective swimming by harnessing vortices through deep reinforcement learning, Proc. Natl. Acad. Sci. USA **115**, 5849 (2018).

[35] S. L. Brunton, B. R. Noack, and P. Koumoutsakos, Machine learning for fluid mechanics, Annu. Rev. Fluid Mech. **52**, 477 (2020).

[36] P. W. Webb, The swimming energetics of trout, J. Exp. Biol. **55**, 521 (1971).

[37] S. P. Gerry and D. J. Ellerby, Resolving shifting patterns of muscle energy use in swimming fish, PLoS ONE **9**, e106030 (2014).

[38] V. Di Santo, C. P. Kenaley, and G. V. Lauder, High postural costs and anaerobic metabolism during swimming support the hypothesis of a U-shaped metabolism–speed curve in fishes, Proc. Natl. Acad. Sci. USA **114**, 13048 (2017).

[39] B. François, Physical aspects of fish locomotion: An experimental study of intermittent swimming and pair interaction, Doctoral thesis, l'Université de Paris, 2021.

[40] X. Ye, Y. Su, S. Guo, and L. Wang, Design and realization of a remote control centimeter-scale robotic fish, in IEEE/ASME International Conference on Advanced Intelligent Mechatronics (IEEE, New York, 2008).

[41] S. Verma, P. Hadjidoukas, P. Wirth, and P. Koumoutsakos, Multi-objective optimization of artificial swimmers, in Proceedings of 2017 IEEE Congress on Evolutionary Computation (CEC) (IEEE, New York, 2017), pp. 1037–1046.

[42] N. C. Prewitt, D. M. Belk, and W. Shyy, Parallel computing of overset grids for aerodynamic problems with moving objects, Prog. Aerosp. Sci. **36**, 117 (2000).

[43] J. L. van Leeuwen, C. J. Voesenek, and U. K. Müller, How body torque and Strouhal number change with swimming speed and developmental stage in larval zebrafish, J. R. Soc. Interface **12**, 20150479 (2015).